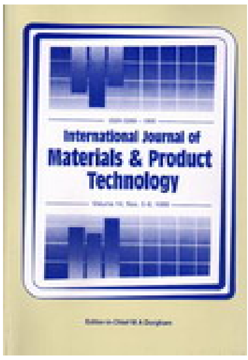


**International Journal of Materials and Product Technology**

ISSN online: 1741-5209 - ISSN print: 0268-1900
https://www.inderscience.com/ijmpt

# Image recognition method of surface defects of prefabricated concrete members in prefabricated building

Zhiyuan Li

**DOI:** 10.1504/IJMPT.2024.10062364

**Article History:**

| | |
|---|---|
| Received: | 25 June 2023 |
| Last revised: | 08 September 2023 |
| Accepted: | 06 November 2023 |
| Published online: | 22 February 2024 |

# Image recognition method of surface defects of prefabricated concrete members in prefabricated building

Zhiyuan Li

School of Construction Engineering,
Chongqing Water Resources and Electric Engineering College,
Yongchuan, Chongqing, 402160, China
Email: 15023152074@163.com

**Abstract:** In view of the cracks, holes and other defects on the surface of prefabricated concrete components in prefabricated building, an Image recognition method of surface defects of prefabricated concrete members in prefabricated building is proposed. This method first performs denoising and enhancement processing on the obtained component defect images to improve the clarity of the images. Based on this, the image is segmented, and the defect features of the component surface defect image are extracted based on the segmentation results. Finally, support vector machines are used to classify the extracted features, achieving accurate recognition of surface defects in prefabricated concrete components. The experimental results show that the recognition effect and accuracy of using this method for component defect image recognition are good.

**Keywords:** prefabricated building; prefabricated concrete members; defect; images recognition.

**Reference** to this paper should be made as follows: Li, Z. (2024) 'Image recognition method of surface defects of prefabricated concrete members in prefabricated building', *Int. J. Materials and Product Technology*, Vol. 68, Nos. 1/2, pp.29–49.

**Biographical notes:** Zhiyuan Li received her PhD from the School of Architecture and Civil Engineering, Taiyuan University of Technology. She is currently working at Chongqing Water Resources and Electric Engineering College. Her research interests include prefabricated buildings, reinforced concrete structures and civil engineering.

## 1 Introduction

In the past half century, China has mainly experienced a period of rapid development in the manufacturing industry. With the unremitting efforts of our technical personnel, management methods and industrial technologies in high-end industrial fields such as automobiles, electronic technology, and aerospace have been continuously innovated, resulting in a significant improvement in the production efficiency of the manufacturing industry. In contrast, the work efficiency and construction quality of China's construction industry are at a low-end level. With the continuous development of society, the demand for reform in the construction industry in the market is gradually increasing. Reforming the extensive design and construction of China's construction industry, improving building efficiency, has become an urgent problem to be solved in China. Since then, the form of prefabricated building (Ji et al., 2021; Chang and Han, 2021) has been proposed and once became the main building form in China, which is widely loved by people. When using prefabricated forms for engineering construction, prefabricated components can usually be divided into concrete prefabricated components, steel structures, and modern wooden structures. Among them, precast concrete components, as key components of the entire building, are the fundamental components of the entire construction process.

During the production process of precast concrete components (Luo et al., 2021; Jian et al., 2021), due to natural and artificial influences, there are defects on the surface of the components, which affect the strength and aesthetic appearance of the concrete components themselves. Therefore, after the completion of the construction of concrete prefabricated components, rapid and accurate surface defect identification becomes one of the necessary inspections for the delivery of concrete prefabricated components. At present, traditional surface defect identification of precast concrete components is mostly carried out through manual detection, which not only has obvious human subjectivity, but also increases the cost loss of manpower. Based on the analysis of the above issues, it is particularly important to propose a simple and efficient method for identifying surface defects in precast concrete components.

Hu et al. (2021) first obtain the texture image of the component, establish a training model, and use human methods to set up missing areas in the image to predict the content of the missing areas; Based on the predicted results, image reconstruction is performed on the surface defect image of the component, and the structural similarity value and residual between the reconstructed image and the image to be tested are calculated; Finally, based on the calculation results of structural similarity values and residuals between images, the detection and recognition of surface defects on components are completed. But the image processing effect of this method is not good. Liu et al. (2022) first establishes a defect recognition model, which is divided into two parts: sample collection and defect recognition. Then, based on the model, feature extraction is performed on the image, and Poisson fusion method is used to fuse the features to generate new image samples. Finally, input the processing results into the defect detection model section, and use this model to achieve surface defect recognition of components. But the recognition accuracy of this method is low. Wang et al. (2022) designed an image recognition method to address the low accuracy of surface defect recognition in traditional detection algorithms. This method first preprocesses the image and performs image non-destructive testing based on the processing results; Then, the intuitionistic fuzzy C-means clustering method is used to perform clustering segmentation on the image, extract image feature values, and determine image feature edges. Finally, defect recognition of the image is achieved through the classification and processing of feature values. But the recognition efficiency of this method is low.

The above surface defect recognition methods failed to carry out necessary image enhancement processing on the defect image in the process of component surface defect recognition, resulting in that the defect recognition effect of the above methods is not obvious during defect detection. Based on the problems in the above defect recognition methods, an image recognition method of surface defects of prefabricated concrete members in prefabricated building is proposed. The specific implementation steps are as follows:

1 Firstly, preprocess the obtained surface texture images of precast concrete components, using anisotropic diffusion equations for denoising, and using Retinex algorithm to enhance the image clarity, thus preparing for the subsequent identification of surface defects in precast concrete components.

2 Secondly, the image is segmented and processed. Based on the segmented image, defect feature points are placed in the image to obtain the pixel values of the feature point positions. The median filtering method is used to perform greyscale processing on the image pixels to obtain the defect features of the component surface defect image.

3 After extracting the surface defect features of prefabricated concrete components, support vector machines (SVMs) are used to classify the extracted features. Based on the classification results, precise recognition of surface defects of prefabricated concrete components in prefabricated buildings is achieved.

4 Through comparative experiments, the denoising effect, image processing effect, feature extraction effect, and recognition effect of the proposed method have been verified to be good, and have practical application value.

## 2 Image preprocessing methods

Before the recognition of the surface defect image of the concrete prefabricated component, the image definition is poor due to the large noise interference of the collected image. Therefore, before the recognition of the surface defect of the concrete prefabricated component of the prefabricated building, the obtained Surface finish image of the concrete prefabricated component needs to be denoised (Lin et al., 2022; Ma et al., 2022) and image enhancement processing (Fu et al., 2022; Panetta et al., 2022) to effectively improve the image definition, prepare for the identification of surface defects in precast concrete components in the future.

### *2.1 Image denoising*

When image denoising is carried out, the anisotropic diffusion equation denoising method is used to complete the surface defect image denoising. Firstly, randomly select a surface finish image of the concrete precast component, set the expression form of the original image as $o(x, y, t)$, and then obtain the main expression form of the diffusion equation. The results are as follows:

$$\begin{cases} \dfrac{\partial o}{\partial t} = div\left[ g\left( |\nabla o| \right) \nabla o \right] \\ o(x, y, 0) = o(x, y) \end{cases} \tag{1}$$

In the equation, the image gradient modulus is expressed in the form of $|\nabla o|$, the diffusion coefficient in the form of $g$, the constant coefficient in the form of $\partial$, the time state in the form of $t$, the image gradient in the form of $\nabla o$, the pixel position in the form of $(x, y)$, and the divergence coefficient in the form of $div$.

Based on the above calculation results, it can be seen that in the diffusion function, the diffusion coefficient determines the diffusion form of the equation. To ensure that the internal details of the image are preserved during image denoising, the coefficient is usually set as a gradient non-negative decreasing function.

The diffusion coefficient (Mahendrakar et al., 2022) is usually described in the form of $g(x) = \frac{1}{1+(x/k)^2}$, where the gradient value is $x$ and the gradient threshold is marked as $k$. When denoising an image, the denoising scale can be determined by the gradient value in the gradient diffusion coefficient. The specific denoising process is as follows:

### 2.1.1 Introduction of diffusion tensor

In noisy images, there is usually a similar structural line with a consistent inclination angle. Therefore, during the denoising process, the direction of the line can be used as the direction of the maximum greyscale change, and the analysis results of the structural tensor can be introduced to achieve the purpose of preserving image details and texture information. By introducing diffusion tensor, the non-diffusive diffusion equation is established as follows:

$$\begin{cases} \dfrac{\partial o}{\partial t} = div[B\nabla o] \\ o(x, y, 0) = o(x, y) \end{cases} \tag{2}$$

In the equation, the matrix type diffusion tensor is expressed in the form of $B$. The matrix expression is as follows:

$$B = \begin{bmatrix} \omega_1 & \omega_2 \end{bmatrix} \begin{bmatrix} b_1 & 0 \\ 0 & b_2 \end{bmatrix} \begin{bmatrix} \omega_1^T \\ \omega_2^T \end{bmatrix} \tag{3}$$

In the formula, the eigenvalue of the expansion tensor is expressed as $b_1$ and $b_2$, the orthogonal eigenvector of the positive-definite matrix is expressed as $\omega_1$ and $\omega_2$, and the incremental function is expressed as $T$.

### 2.1.2 Local forward and reverse diffusion

Based on the above analysis results, when obtaining the diffusion coefficient value based on the image gradient, a small gradient corresponds to a positive diffusion coefficient, and vice versa, it is negative. This can achieve the goal of eliminating noise while preserving image details. The obtained diffusion coefficient is as follows:

$$g(x) \begin{cases} 1-\left(x/k_1\right)^m; & 0 \le x \le k_1 \\ \beta\left(\left((x-k_1)/\omega\right)^{2n}\right)k_{2;} & -\omega \le x \le k_2 + \omega \\ 0; & \text{otherwise} \end{cases} \tag{4}$$

In the equation, the diffusion direction is expressed in the form of $k_1$ and $k_2$, the diffusion intensity is expressed in the form of $m$ and $n$, the diffusion weight is expressed in the form of $\omega$, the image gradient is expressed in the form of $x$, the diffusion coefficient is expressed in the form of $g(x)$, and the constant is described in the form of $\beta$. When the pixel gradient of the image is at $[k_{2-\omega}, k_{2+\omega}]$ and the diffusion coefficient is negative, it is necessary to reverse diffuse the image to sharpen it; If the image gradient is greater than $k_{2+\omega}$, then the diffusion coefficient is 0 and the pixels are not expanded for diffusion.

### *2.1.3 Establishment of diffusion forms*

Due to the fact that the feature vectors of the diffusion tensor and the structural tensor are both ω, and the feature vectors can locate the edge direction of the image, effectively ensuring the gradient edge direction of pixel diffusion. Therefore, the feature vector can be fixed in a certain range, and the diffusion equation for image denoising can be re-established according to the diffusion tensor and diffusion coefficient determined above. The results are as follows:

$$\frac{\partial o}{\partial t} = b_1 \frac{\partial^2 o}{\partial^2 \omega} + b_2 \frac{\partial^2 o}{\partial^2 \omega_2} \tag{5}$$

where the reconstructed diffusion equation is expressed in form $\frac{\partial o}{\partial t}$.

From the observation of the above equation, it can be seen that the diffusion intensity of noisy images in the gradient direction is denoted as $b_1$ form, and the diffusion intensity in the edge direction is expressed as $b_2$ form. When image diffusion occurs, the gradient direction is usually fixed, and only diffusing the image towards the edge direction will increase the impact of noise in the image denoising process. To avoid this problem, it is necessary to consider the gradient information in the texture image into the noise and redefine $b_1$ and $b_2$. The idea of local forward and backward diffusion is integrated into the noise, and the gradient value of the image texture line structure is set within the range of $[k_1, k_2]$, and the image noise is defined as the gradient less than $k_1$ and greater than $k_2$. The image noise is directly eliminated, so as to realise the denoising of the texture image of the prefabricated concrete components of Prefabricated building.

## *2.2 Image enhancement processing*

After denoising the surface image of concrete prefabricated components, the defect edges in the image are still unclear. Therefore, before image segmentation, it is necessary to use the retinex algorithm (Sun et al., 2021; Kong et al., 2021) based on the denoising results to enhance the image.

Based on the retinex theory, the precast concrete component is set as the product of the illumination image and the reflection image to obtain the mathematical expression of the surface defect image of the precast concrete component. The results are shown in the following equation:

$$S(x, y) = R(x, y) * L(x, y) \tag{6}$$

In the formula, the surface defect image of the concrete prefabricated component after denoising is expressed in the form of $S(x, y)$, the illumination image is expressed in the form of $L(x, y)$, and the reflection image is recorded as $R(x, y)$. Among them, reflection image is the essential attribute, and illumination image represents the dynamic range of the image. The essence of image enhancement is to obtain the essential attributes of the image from the original image, in order to avoid the influence of illumination on the image and achieve colour constancy. The specific image enhancement process is shown in Figure 1.

**Figure 1** Enhancement flowchart in the image

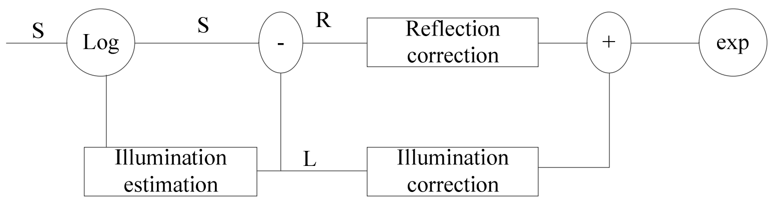


### 2.2.1 *Image illuminance estimation*

When estimating the illuminance of the surface defect image of the concrete prefabricated component, set the pixel set of the image as $\varphi$, and express the Gaussian function of the image in the form of $f$, $h$, so as to obtain the bilateral filtering results of the image pixel points. The process is as follows:

$$\begin{cases} D_S = \dfrac{1}{\gamma(S)} \sum_{u\in\varphi} f(u-s)h(I_u - I_s) I_u \\ \gamma(S) = \sum_{u\in\varphi} f(u-s)h(I_u - I_s) \end{cases} \tag{7}$$

In the formula, the brightness value of point $u$ in the image is expressed in the form of $I_u$, the standardisation factor is expressed in the form of $\gamma(S)$, the brightness value of pixel s in the image is expressed in the form of $I_s$, and bilateral filtering results of image pixels are described in $D_S$. According to the above calculation results, it can be seen that the brightness value of pixels in the image will be affected by adjacent similar brightness pixels. Therefore, in specific image illuminance estimation, it is necessary to use greyscale value layering algorithm to improve the calculation speed of bilateral filtering. The specific illuminance estimation process is as follows:

1 Firstly, the denoised surface defect image of the precast concrete component is set as a two-dimensional image to complete the initialisation of the image vector grid. The process is as follows:

$$\vartheta\left(u_x, u_y, \delta\right) = \begin{cases} \left(I(u_x, u_y), 1\right); & \text{if } \delta = I\left(u_x, u_y\right) \\ (0, 0, 0); & \text{otherwise} \end{cases} \tag{8}$$

In the equation, the initialisation result of the image vector grid is expressed in the form of $\vartheta(u_x, u_y, \delta)$, the pixel position is expressed in the form of $(u_x, u_y)$, the brightness value of the pixel is expressed in the form of $I(u_x, u_y)$, the vector grid is described in the form of $\vartheta$, and the reflection value of the pixel is expressed in the form of $\delta$.

2 Based on the initialisation results of the image vector grid mentioned above, Gaussian filtering is applied to the grid, and the processing process is as follows:

$$E[\vartheta]\left(u_x, u_y, \delta\right) = G_{\eta_s,\eta_r} * \vartheta\left(u_x, u_y, \delta\right) \quad (9)$$

In the formula, the three-dimensional Gaussian function is expressed in form $G_{\eta_s,\eta_r}$, the spatial domain parameters of the image are expressed in form $\eta_s$, the luminance domain coefficients are expressed in form $\eta_r$, and the Gaussian filtering results of the image are expressed in form $E[\vartheta](u_x, u_y, \delta)$.

3 Based on the Gaussian processing results of the above images (Gu et al., 2021; Li et al., 2022), the pixel $(u_x, u_y, I_u)$ position is set in the image grid vector to implement bilateral filtering processing, in order to obtain the estimated illuminance values of the surface defect images of concrete prefabricated components.

### *2.2.2 Illumination image compression*

After completing the illumination estimation, the pixels on both sides of the image illumination histogram are intercepted through histogram capture, and the remaining pixels are compressed to the range of [0, 1]. The improved gamma correction algorithm is used to correct the pixels, thereby obtaining the final illumination image. During the process, the original pixel value of the component surface defect image is set to $i$, and the control parameter is set to $\psi$. The correction results of the image pixels are shown in the following equation:

$$\theta(i) = i^{\psi * i + \psi} \quad (10)$$

In the formula, the correction result of image pixels is expressed in the form of $\theta(i)$.

The pixel correction results are shown in Figure 2.

**Figure 2** Pixel correction results

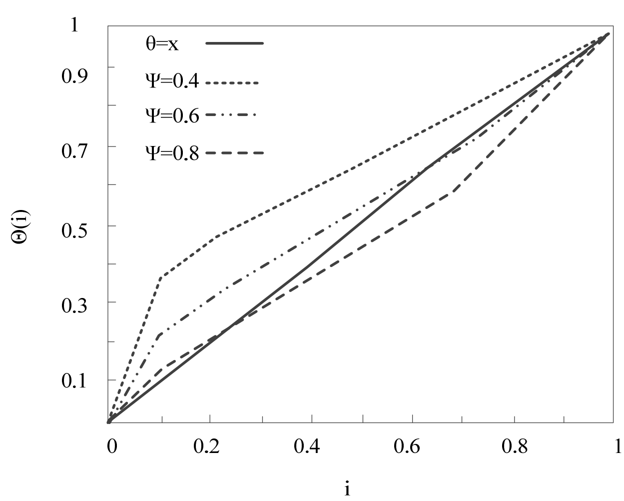


Analysing Figure 2, it can be seen that when adjusting the correction function by adjusting the coefficient, the smaller the adjustment coefficient, the more effective the overall brightness adjustment of the image. When the adjustment parameter is 0.6, the pixel values of the lower pixels in the image are approximately above function $\theta = x$, and a small portion of the pixel values are below function $\theta = x$. This indicates that during pixel correction, the low brightness areas in the image can be enhanced, effectively suppressing overexposure in high brightness areas. When adjusting the parameter to 0.8, it can be seen that the small and low pixels in the image are above function $\theta = x$, and the majority of pixel values are below $\theta = x$, indicating that this curve has better compression effect on images with higher brightness.

### *2.2.3 Reflection component enhancement*

After obtaining the illumination image of the surface defect image of precast concrete components, it is necessary to perform a difference operation between the original image and the illumination image in the numerical domain to obtain the reflection component of the component defect image. During the process, the control coefficient is set to ɩ to obtain the reflection component value of the image, and the result is as follows:

$$f(r) = \frac{2}{1+\mu^{-\iota * r}} - 1 \tag{11}$$

In the formula, the reflection brightness of the image is expressed in the form of $r$, the obtained reflection component values of the image are described in the form of $f(r)$, and the increment function is recorded in the form of $\mu^{-\iota * r}$. The brightness mapping of the reflection image of component surface defects is shown in Figure 3.

**Figure 3** Brightness mapping of component surface defect reflection images

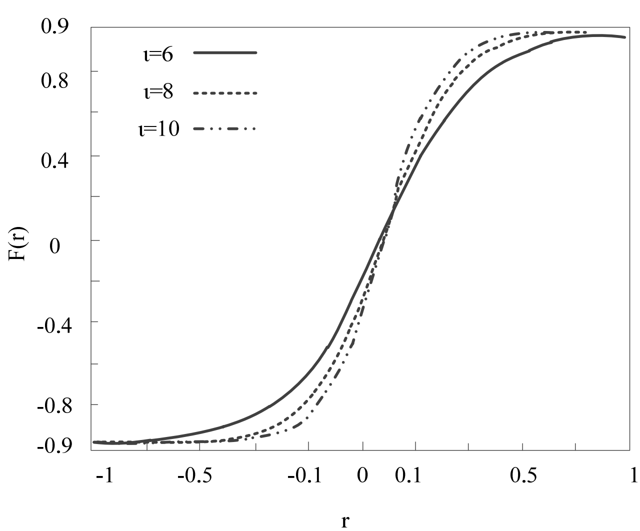


Analysing Figure 3, it can be seen that the steeper the mapping curve, the more significant the image enhancement effect. The specific image enhancement process is as follows:

1. According to the RGB channel component value of the image, obtain the brightness image of the component image, select the appropriate logarithm, and use the bilateral filtering algorithm to determine the image illuminance component.
2. Calculate the difference between the illuminance component and the brightness component of the image, determine the reflection component value of the image, and combine it with the histogram capture algorithm to capture 1% of the pixels at both ends of the image, and use the pixel correction equation to correct them.
3. After completing the correction, recalculate the image reflection brightness value, combined with the determined image illuminance value, obtain a new component surface defect image, and complete the image enhancement processing.

## 3 Image recognition method for surface defects of precast concrete components

Based on the above image preprocessing results, the image is segmented (Li et al., 2022; Ji et al., 2022), and the defect features of the component surface defect image are extracted based on the segmentation results. Finally, SVMs are used to classify and process the extracted features, thereby achieving accurate recognition of surface defects in prefabricated concrete components.

### *3.1 Image segmentation*

Firstly, based on the image processing results, the greyscale range of the image is set to be within $[0, 1, \cdots, \xi - 1]$, and the number of pixels with a greyscale value of $i$ is expressed in the form of $m_i$, while the total number of pixels in the image is described in the form of $M$. This obtains the probability of $m_i$ appearing in the image, $\rho_i$, and divides it into two categories using an appropriate threshold to calculate the probabilities of different pixel values $P_0(t)$ and $P_1(t)$. The overall greyscale value of the image is obtained, and the inter class variance of different categories of the image is determined as follows:

$$\bar{L} = P_0(t)\left[(t)_0 - T_-\right]^2 + P_1(t)\left[(t)_{-1} - T_-\right]^2 \tag{12}$$

In the formula, the overall greyscale value of the image is expressed in the form of $T_-$, the inter class variance of the obtained image is expressed in the form of $\bar{L}$, and the pixel greyscale probability coefficient is expressed in the forms of $(t)_0$ and $(t)_1$.

By selecting the optimal segmentation threshold for the surface defect image of concrete components based on the determined inter class variance, the image segmentation is completed. The process is as follows:

$$YZ = \arg\max_{0<t<-1} \bar{L}(t) \tag{13}$$

In the formula, the segmentation threshold of the image is expressed in the form of $YZ$, the maximum inter class variance is expressed in the form of $\max_{0<t<-1}$, and the variable function is described in the form of arg.

### 3.2 Image defect feature extraction

Based on the above image segmentation results, defect feature points are placed in the image to obtain the pixel values of the feature point positions. The median filtering method (Hyun et al., 2021; Meng et al., 2021) is used to perform greyscale processing on the image pixels to obtain the defect greyscale features of the image. This method can effectively remove noise and pseudo defects, and improve the accuracy of feature extraction. By extracting features such as greyscale mean, variance, contrast, energy, information entropy, and maximum and minimum pixel greyscale values from surface defect images of precast concrete components, the greyscale distribution and texture features of defects can be better described, and the accuracy and robustness of recognition can be improved. The specific feature extraction process is shown in Figure 4.

**Figure 4** Defect feature extraction process

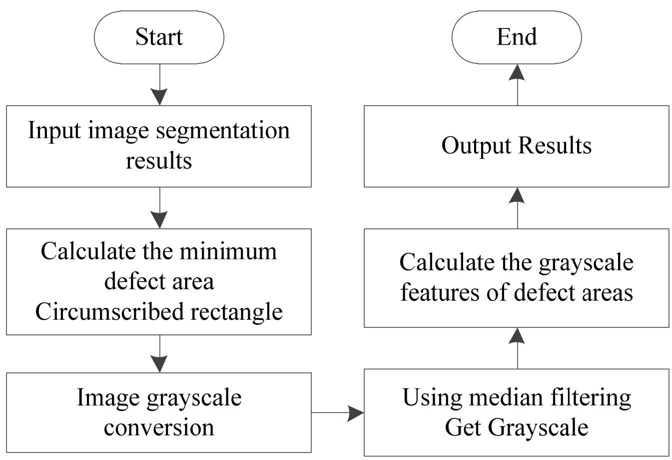


The feature extraction algorithm is one of the cores of defect recognition, and the extraction effect of defect features can directly affect the recognition accuracy of defect recognition. Due to the presence of some noise points and pseudo defects on the surface of precast concrete components after the completion of the troweling process, it interferes with identification. Therefore, it is particularly important to perform noise removal and image enhancement before obtaining the greyscale defect features of the image. Based on the segmentation processing results of the enhanced image mentioned above, the greyscale histogram of the image is used as the defect feature vector value, and the number of pixels with a greyscale value of µ is set to $m(\mu)$, and the total number of pixels is expressed as $M$. In this way, the greyscale histogram of the segmented image is obtained, as shown in the following equation:

$$HD(\mu) = m(\mu) / M \tag{14}$$

In the formula, the greyscale quantisation level of the image is expressed in the form of $\mu$, and the obtained greyscale histogram of the image is described in the form of $HD(\mu)$.

Based on the determined greyscale histogram of the image, the defect features of the image are extracted, and the process is as follows:

$$\begin{cases} HD_{jz} = \sum_{\mu=0}^{M} \mu HD(\mu) \\ \sigma^2 = \sum_{\mu=0}^{M} (\mu - \overline{\mu})^2 HD(\mu) \\ HD_{db} = \max \phi(i, j) - \min \phi(i, j) \\ NL_{HD} = \sum_{\mu=0}^{M} HD(\mu)^2 \\ SZ = \sum_{\mu=0}^{M} HD(\mu) \log_2 \left( HD(\mu) \right) \end{cases} \tag{15}$$

In the formula, the average grey level of the extracted surface defect images of concrete prefabricated components is expressed in the form of $HD_{jz}$, the grey level variance is expressed in the form of $\sigma^2$, the grey level contrast of the image defect position is expressed in the form of $HD_{db}$, the energy of the image defect position is expressed in the form of $NL_{HD}$, the information entropy is expressed in the form of $SZ$, the maximum pixel grey level value of a pixel is expressed in the form of $\max\phi(i, j)$, and the minimum pixel grey level value is expressed in the form of $\min\phi(i, j)$.

### *3.3 Image recognition method for surface defects of components*

SVM is a supervised learning algorithm that performs well in classification problems. It is based on statistical learning theory and the principle of structural risk minimisation, which separates data samples of different categories by finding an optimal hyperplane. This enables SVM to have good performance in handling both binary and multi classification problems. It has the advantages of robustness, ability to handle high-dimensional spatial data, strong generalisation ability, and effectiveness for small sample data. By using SVM, the surface defects of precast concrete components can be accurately classified and identified based on the extracted defect features. Therefore, after extracting the surface defect features of prefabricated concrete components, SVMs (Yu et al., 2022; Zou et al., 2021) are used to classify the extracted features, and based on the classification results, accurate recognition of surface defects of prefabricated concrete components in prefabricated buildings is achieved.

When using SVM for image defect feature classification, it is essentially searching for an optimal classification surface that can separate two types of samples and maximise the classification interval between the two types of samples.

Firstly, set the training sample set as $[x_i, y_i]_{i-1}^{M}$ according to the component defect image obtained above, where the $i$ sample under the vector machine input mode is expressed as $x_i$, the sample variable is expressed as $y_i$, the hyperplane equation is set as $W^T X + b = 0$, the plane normal vector is expressed as $W$, and the constant term is expressed as $b$. Based on the above set values, obtain the distance between two boundary lines to complete the optimal classification surface of the vector machine, as shown in the following equation:

$$\begin{cases} Dis = d_1 + d_2 = \dfrac{2}{\| W \|} \\ \begin{cases} \min v(w) = \dfrac{1}{2} \| W \|^2 = \dfrac{1}{2} (w^T w) \\ s.t. \; y_i \left( w^T x_i + b \right) - 1 \geq 0 \end{cases} \end{cases} \tag{16}$$

In the formula, the distance between the boundary and the upper boundary of the SVM is expressed in the form of $d_1$, the distance from the boundary to the lower boundary is expressed in the form of $d_2$, the maximum distance between the boundaries is expressed in the form of *Dis*, the best obtained boundary is described in the form of min$v(w)$, and the constraint conditions are expressed in the form of s.t.

Finally, through the best classification surface found, the establishment of the SVM is completed. After the establishment of the SVM, the component defect features in the original space are mapped to the high-dimensional space of the vector machine through the kernel function, so as to complete the accurate classification of surface defects of prefabricated concrete components of Prefabricated building. The results are shown in the following formula:

$$f(x) = K\left(x_i, y_j\right) * \min v(w) \left[ y_i \left( w^T x_i + b \right) \right] \varpi \tag{17}$$

In the formula, the classification results of component defect features are expressed in the form of $f(x)$, the classification weights are expressed in the form of $\varpi$, and the kernel function is expressed in the form of $K(x_{\mathrm{i}}, y_j)$.

## 4 Experiment

In order to verify the overall effectiveness of the image recognition method for defects in precast concrete components mentioned above, it is necessary to test this method. In the experiment, a camera or professional image acquisition equipment was used to capture the surface of precast concrete components, and the image data was obtained to form dataset 1. Simultaneously obtain partial images from the common objects in context (COCO) database to form dataset 2. Mix two datasets to form a mixed dataset as the initial data. Select 200 surface images of concrete components as the initial image data. This dataset contains different types and degrees of concrete cracks, with 1500 samples. The size of each image is 256 × 256 pixels and has been annotated by professionals to indicate the location and type of cracks in each image. Divide the dataset into training and testing sets, with 70% of the images used to train the model and 30% used to evaluate the accuracy of the model. During the testing process , comparative tests were carried out on the research of image recognition methods for surface defects of prefabricated concrete components of prefabricated building (the proposed methods), unsupervised surface defect detection methods based on inpainting [method of Hu et al. (2021)], workpiece surface defect detection methods oriented to unbalanced sample space [method of Liu et al. (2022)], and aluminium surface defect detection methods based on improved faster RCNN [method of Wang et al. (2022)], verify the practical application feasibility of the proposed defect image recognition method.

## *4.1 Protocol*

During the testing process, in order to verify the effectiveness of different methods in identifying defects, a prefabricated component processing factory in a certain city was selected to collect surface defect images of concrete prefabricated components on site. The proposed method, method of Hu et al. (2021), method of Liu et al. (2022), and method of Wang et al. (2022) were used for defect image recognition, and the denoising and processing effects of the images were evaluated the specific test results of image feature extraction performance and actual recognition performance verify the actual effectiveness of different methods in defect image recognition process.

## *4.2 Acquisition of experimental indicators*

The indicators used in the above experimental plan are as follows:

In the process of image denoising, the denoising performance of different methods is evaluated from both subjective and objective aspects. The visual effect of the denoised image is scored and ranked based on subjective evaluation, and the average score is calculated. In order to avoid the subjective influence of the observer during the process, Z-scores were used to compare the subjective denoising effects of different algorithms. The Z-score calculation process is shown in the following equation:

$$Z = \frac{X - \bar{X}}{\varepsilon} \tag{18}$$

In the formula, the subjective score is described in the form of $X$, the average score in the form of $\bar{X}$, and the standard deviation in the form of $\varepsilon$.

When objectively evaluating the denoising effect, peak signal-to-noise ratio, structural similarity, and image information entropy are selected as test indicators. The acquisition process is as follows:

$$\begin{cases} Q_{PSNR} = 20 \lg\left(\dfrac{255}{L_{MSE}}\right); L_{MSE} = \sqrt{\dfrac{1}{MN}\sum_i (o_i - o_{1i})^2} \\ SSIM(x, y) = \dfrac{(2a_x a_y + c_1)(2\varepsilon_{xy} + c_2)}{(a_x^2 + a_y^2 + c_1)(\varepsilon_x^2 + \varepsilon_y^2 + c_2)} \\ E_{ntropy} = -\sum q(x) \log_2 q(x) \end{cases} \tag{19}$$

In the formula, the horizontal and vertical scales of the component surface defect image are expressed in MN form, the original image is expressed in $o_i$ form, the denoised image is expressed in $o_{1i}$ form, the peak signal-to-noise ratio is expressed in $Q_{PSNR}$ form, the structural similarity is expressed in $SSIM(x, y)$ form, the information entropy is expressed in $E_{ntropy}$ form, the image covariance is described in $\varepsilon$ form, the mean is expressed in a form, the image pixel value is described in $x$, $y$ form, the relative frequency machine is described in $q(x)$ form, and the constants are recorded in $q(x)$ and $c_2$.

And conduct testing on the recognition effect of component surface defects, using recognition accuracy, recognition time, and actual application effect as test indicators to test the recognition effect of the proposed method, proposed method, method of Hu et al. (2021), method of Liu et al. (2022), and method of Wang et al. (2022) defect image recognition. The recognition accuracy evaluation indicators are accuracy. The recall rate is used to verify the specific recognition performance of the proposed method in image recognition.

## 4.3 Experimental results

### 4.3.1 Noise reduction effect test

When using the proposed method, method of Hu et al. (2021), method of Liu et al. (2022), and method of Wang et al. (2022) for defect image recognition, the image processing effects of different methods in image recognition were tested using the relevant evaluation indicators obtained above. The test results are shown in Table 1.

**Table 1** Test results of denoising effects of different methods

| *Number of images to be recognised/piece* | *Test indicators* | *Test results of denoising effect* | | | |
|---|---|---|---|---|---|
| | | *Proposed method* | *Method of Hu et al. (2021)* | *Method of Liu et al. (2022)* | *Method of Wang et al. (2022)* |
| 50 | Z score | 1.33 | 0.71 | 0.19 | -0.03 |
| | $Q_{PSNR}$ | 42.55 | 40.34 | 39.98 | 98.25 |
| | $SSIM(x, y)$ | 1.12 | 1.10 | 1.08 | 1.06 |
| | $E_{ntropy}$ | 7.61 | 7.55 | 7.21 | 7.06 |
| 100 | Z score | 1.31 | 0.68 | 0.16 | -0.035 |
| | $Q_{PSNR}$ | 40.38 | 38.66 | 36.73 | 35.99 |
| | $SSIM(x, y)$ | 1.12 | 0.99 | 0.96 | 0.95 |
| | $E_{ntropy}$ | 7.58 | 7.36 | 7.01 | 6.92 |
| 150 | Z score | 1.28 | 0.61 | 0.05 | -0.042 |
| | $Q_{PSNR}$ | 38.25 | 36.19 | 34.25 | 32.98 |
| | $SSIM(x, y)$ | 1.08 | 0.95 | 0.92 | 0.88 |
| | $E_{ntropy}$ | 7.47 | 7.18 | 6.79 | 6.55 |
| 200 | Z score | 1.25 | 0.22 | -0.01 | -0.055 |
| | $Q_{PSNR}$ | 35.98 | 33.44 | 31.85 | 29.71 |
| | $SSIM(x, y)$ | 1.06 | 0.91 | 0.88 | 0.84 |
| | $E_{ntropy}$ | 7.36 | 6.94 | 6.66 | 6.34 |
| 250 | Z score | 1.18 | 0.05 | -0.033 | -0.14 |
| | $Q_{PSNR}$ | 33.79 | 31.47 | 29.43 | 27.91 |
| | $SSIM(x, y)$ | 1.01 | 0.87 | 0.83 | 0.79 |
| | $E_{ntropy}$ | 7.25 | 6.71 | 6.51 | 6.28 |

When denoising an image, based on the above evaluation indicators, it can be concluded that the higher the peak signal-to-noise ratio, structural similarity, and image information entropy of the denoised image, the better the denoising effect of the method. According to Table 1, when denoising component defect images, the proposed method measures the best values of various indicators among the four methods. This can prove that the proposed method has high denoising performance in image denoising. According to the test results in Table 1, the above four methods were applied to actual image defect recognition to detect the actual image denoising effect of the four methods in defect recognition. The results are shown in Figure 5.

**Figure 5** Test results of denoising effects of different methods (see online version for colours)

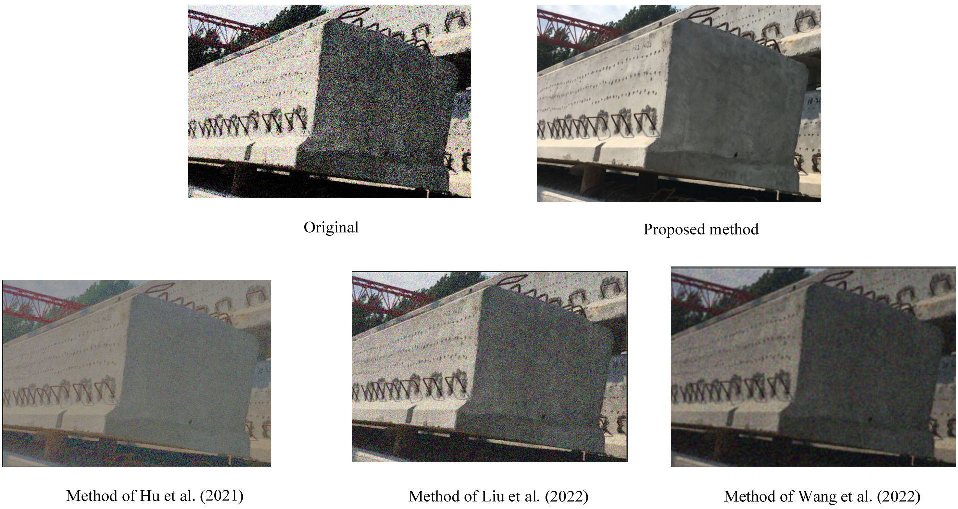


During the process of identifying surface defects in components, there is a large amount of noise in the image. If the image cannot be denoised in a timely manner, it will directly affect the accuracy of subsequent image defect recognition. Analysing Figure 5, it can be seen that the denoising effect of the proposed method is the best among all methods in image defect recognition. This is because the proposed method uses anisotropic diffusion equations, which is a commonly used image denoising method that smoothes the image by calculating the gradient of each pixel in the image, thereby removing noise. This method effectively reduces the impact of noise on image quality while maintaining image edge information. Among them, method of Hu et al. (2021) used unsupervised model expansion for image denoising during defect recognition. Due to the low performance of unsupervised model denoising, the denoising effect of this method is not ideal. Method of Liu et al. (2022) and method of Wang et al. (2022) both have certain effects on image denoising, but the denoising effect of the two methods in image defect recognition is lower than that of the proposed method.

### *4.3.2 Image processing effect testing*

When using the proposed method, method of Hu et al. (2021), method of Liu et al. (2022), and method of Wang et al. (2022) for defect image recognition, the image processing effects of different methods in image recognition were tested. The test results are shown in Figure 6.

When identifying surface defects on components, the clarity of the captured images is usually poor due to the influence of surrounding environmental factors. As a key link in image defect recognition, image processing is an important part that determines the actual recognition effect of component surface defects. The better the image processing effect, the better the recognition effect of surface defects on subsequent components, and vice versa. Analysing Figure 6, it can be seen that the image processing effect of the proposed method is the best among the four methods for identifying surface defects of components. This is mainly because the proposed method not only effectively denoises the image during the image processing process, but also timely enhances the denoised image, improving the clarity of the image. Therefore, this method has good image processing effect in defect recognition.

**Figure 6** Test results of image processing effects using different methods (see online version for colours)

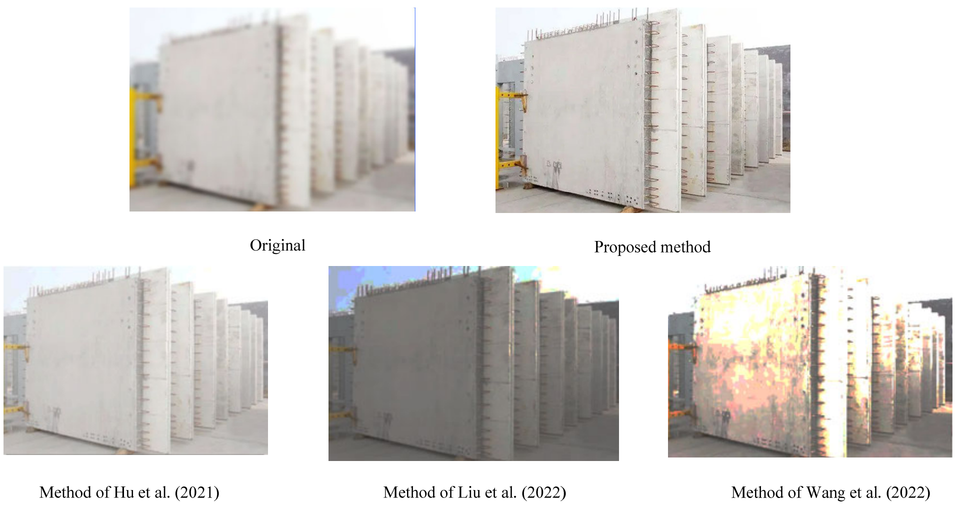


### *4.3.3 Testing the effectiveness of image feature extraction*

Based on the above test results, we will continue to use the proposed method, method of Hu et al. (2021), method of Liu et al. (2022), and method of Wang et al. (2022) for defect image recognition. During the image feature extraction process during image recognition, we will conduct tests on the key feature pixels of defects determined by different methods. The test results are shown in Figure 7.

In the process of identifying surface defects on components, it is necessary to extract the defect features of the component defect image. The accuracy of feature extraction can directly reflect the effectiveness of image defect recognition. If the number of key feature points extracted from the image is small, it will directly reduce the accuracy of defect recognition. Analysing Figure 7, it can be seen that method of Wang et al. (2022) has the lowest number of key feature points obtained in the image among the four methods for extracting defect features. Therefore, this method has poor feature extraction performance when extracting defect features. Method of Hu et al. (2021) and method of Liu et al. (2022) have certain effects on image processing, so the pixel points of defect positions obtained by the two methods for image defect feature extraction are only lower than the test results of the proposed method. As the proposed method has the best image processing performance among the four methods, the distribution values of the key pixel points at the defect location obtained by this method are consistent with the expected key defect pixel points when extracting image defect features. This is because the proposed method uses segmentation technology to process the image and places defect feature points in the image. By obtaining the position and pixel value of the feature points, and combining with median filtering method for greyscale processing, the key features of component surface defects are effectively captured. This proves that the proposed method extracts more accurate feature values when extracting surface defect features of components.

**Figure 7** Test results of image feature extraction effects using different methods (see online version for colours)

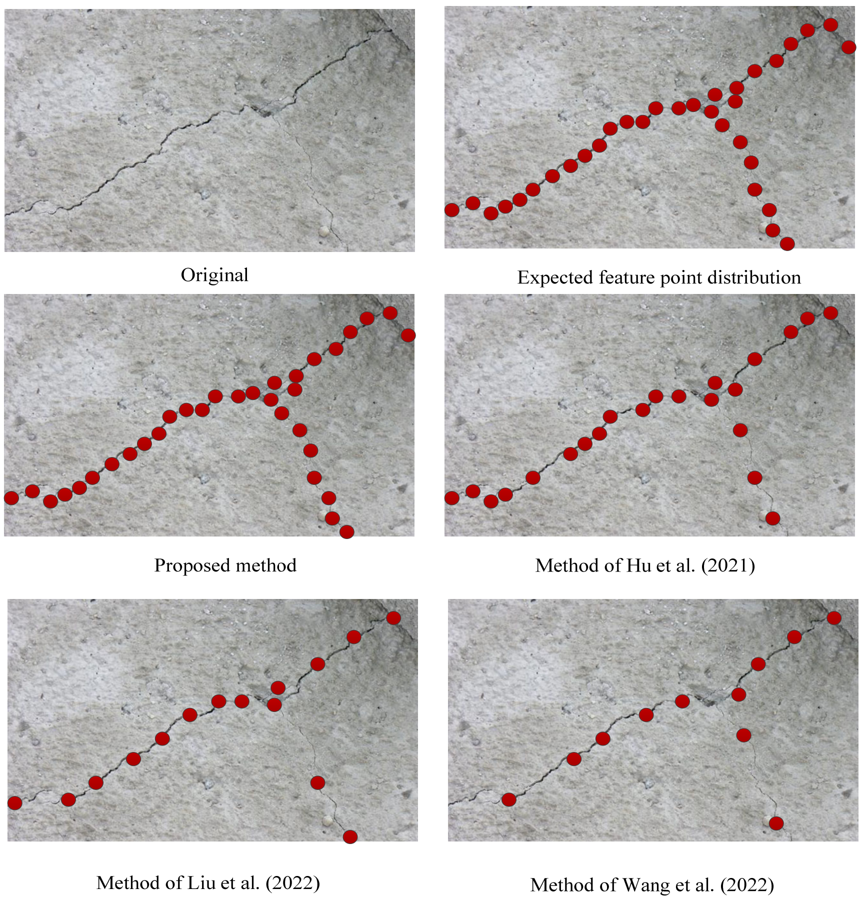


### *4.3.4 Recognition effect test*

When using the proposed method, method of Hu et al. (2021), method of Liu et al. (2022), and method of Wang et al. (2022) for defect image recognition, the recognition accuracy and recognition time of different methods in image recognition were tested. The test results are shown in Table 2.

When identifying surface defects on components, the test results of recognition accuracy and recovery rate can intuitively reflect the recognition performance of the recognition method. According to Table 2, as the number of images to be identified increases, the four methods tested show a varying degree of decline in recognition accuracy and recall index values when identifying surface defects on components. The recognition time also increases with the increase of the number of images. Among them, method of Hu et al. (2021) reconstructed surface defect images, and there were significant errors in calculating the structural similarity values and residuals between the reconstructed image and the detected image. Therefore, the recognition accuracy and recognition time of this method in image defect recognition were lower than the test results of the proposed method. Method of Liu et al. (2022) had problems implementing image fusion based on Poisson fusion method, so the recognition accuracy, recall rate, and recognition time of this method in image defect recognition were slightly lower than the proposed method and the test results of method of Hu et al. (2021). Due to the failure to consider the impact of noise on clustering during the defect clustering process of method of Wang et al. (2022), the recognition accuracy, recall rate, and recognition time of this method in image defect recognition are all the worst among the four methods. The proposed method, due to the timely implementation of enhancement processing on the obtained images before image defect recognition, effectively improves the clarity of the images. Therefore, the recognition accuracy and recall rate tested by this method during defect recognition are the highest among the four methods, and the detection recognition time is lower than the test results of the other three methods.

**Table 2** Identification accuracy test results of different methods

| *Number of images to be recognised/piece* | *Test indicators* | *Identification accuracy test results* | | | |
|---|---|---|---|---|---|
| | | *Proposed method* | *Method of Hu et al. (2021)* | *Method of Liu et al. (2022)* | *Method of Wang et al. (2022)* |
| 100 | Accuracy/% | 100 | 100 | 99.97 | 99.95 |
| | Recall rate/% | 100 | 99.98 | 99.64 | 99.33 |
| | Recognition time/ms | 25 | 26 | 27 | 28 |
| 200 | Accuracy/% | 100 | 99.94 | 99.63 | 99.45 |
| | Recall rate/% | 100 | 99.01 | 98.78 | 98.67 |
| | Recognition time/ms | 28 | 30 | 33 | 35 |
| 300 | Accuracy/% | 99.99 | 99.25 | 98.86 | 98.44 |
| | Recall rate/% | 99.87 | 98.73 | 98.21 | 97.82 |
| | Recognition time/ms | 32 | 35 | 40 | 46 |
| 400 | Accuracy/% | 98.85 | 98.57 | 98.22 | 97.95 |
| | Recall rate/% | 97.94 | 98.11 | 97.57 | 97.39 |
| | Recognition time/ms | 36 | 40 | 45 | 52 |
| 500 | Accuracy/% | 98.23 | 97.14 | 96.99 | 96.31 |
| | Recall rate/% | 97.99 | 97.64 | 97.05 | 96.94 |
| | Recognition time/ms | 40 | 51 | 55 | 60 |

Based on the above test results, the proposed method, method of Hu et al. (2021), method of Liu et al. (2022), and method of Wang et al. (2022) were applied to the actual recognition of surface defects in concrete components to test the actual recognition effectiveness of the four methods mentioned above. The results are shown in Figure 8.

**Figure 8** Test results of actual defect recognition effects using different methods (see online version for colours)

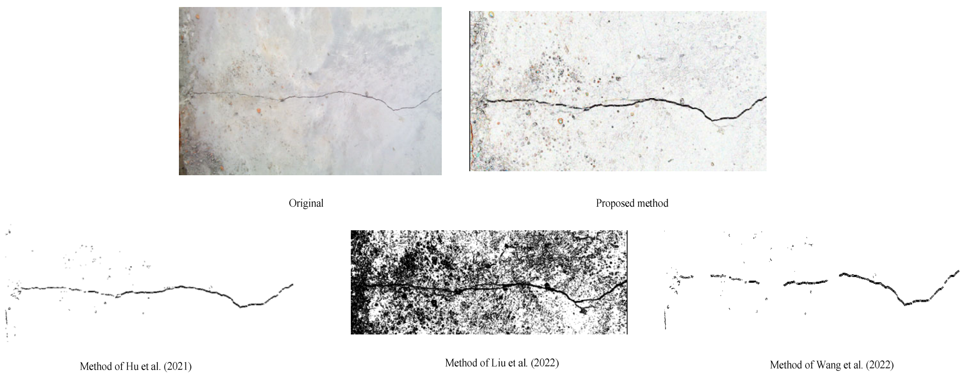


It can be seen from the analysis of Figure 8 that the recognition effect of the proposed method is the best of the four methods when carrying out image recognition of surface defects of prefabricated concrete components of Prefabricated building, so this method can completely detect the shape of defects when identifying defects, while the recognition effect of the other three methods is significantly lower than the recognition effect of the proposed method when identifying defects. This is because the proposed method uses SVM as a classifier for feature classification processing, which has good classification performance and generalisation ability. By providing sufficient training samples and optimising parameters, the accuracy and robustness of the classifier can be improved.

To sum up, the proposed method is used to carry out image recognition of surface defects of prefabricated concrete components in prefabricated building, with good recognition effect and high performance.

## 5 Conclusions

With the gradual increase of the application scope of prefabricated building in engineering construction, it is particularly important to implement surface defect recognition for the concrete components required by prefabricated building. Aiming at the problems existing in the traditional recognition methods, this paper proposes the research on the image recognition method of surface defects of prefabricated concrete components in prefabricated building. This method first preprocesses the surface defect images of precast concrete components obtained. Based on the processing results, the grey level feature extraction method is used to extract the defect features. Finally, the SVM method is used to accurately classify the features, thus achieving accurate recognition of defect images. The experimental results show that the proposed method has a high Z-score value, good denoising effect, clearer image enhancement effect, high accuracy in defect feature extraction, high recognition accuracy and recall rate, fast recognition efficiency, and good recognition effect. Therefore, the proposed method has certain practical application value and can solve the defects of traditional surface defect recognition methods. Due to certain issues with this method in image feature extraction, we will continue to optimise the recognition method in the future to address this issue.

## References


Chang, C. and Han, M. (2021) 'Production scheduling optimization of prefabricated building components based on DDE algorithm', *Mathematical Problems in Engineering*, Vol. 32, No. 5, pp.1–11.

Fu, Y., Hong, Y., Chen, L. et al. (2022) 'LE-GAN: unsupervised low-light image enhancement network using attention module and identity invariant loss', *Knowledge-based Systems*, 15 March, Vol. 240, No. 25, pp.1–11.

Gu, Q.Q., Lü, S-s., Jiang, M.S. et al. (2021) 'Phase error correction method based on the Gaussian filtering algorithm and intensity variance', *Optoelectronics Letters*, Vol. 17, No. 4, pp.221–225.

Hu, G., Wang, N., He, W. et al. (2021) 'Unsupervised surface defect detection method based on image in painting', *Journal of South China University of Technology (Natural Science Edition)*, Vol. 4, No. 7, pp.76–85+124.

Hyun, J., Kim, Y., Kim, J. et al. (2021) 'Hardware-friendly architecture for a pseudo 2D weighted median filter based on sparse-window approach', *Multimedia Tools and Applications*, Vol. 80, Nos. 26/27, pp.21–36.

Ji, B., Hu, X., Ding, F. et al. (2022) 'An effective color image segmentation approach using superpixel-neutrosophic C-means clustering and gradient-structural similarity', *Optik*, Vol. 260, No. 1, pp.169039–169059.

Ji, Y., Zhao, Z., Yao, F. et al. (2021) 'Factors influencing sleeve grouting quality for prefabricated building: an interpretive structural modeling approach', *Advances in Civil Engineering*, Vol. 12, No. 13, pp.1–15.

Jian, S.M., Wu, B. and Hu, N. (2021) 'Environmental impacts of three waste concrete recycling strategies for prefabricated components through comparative life cycle assessment', *Journal of Cleaner Production*, Vol. 328, No. 15, pp.1–11.

Kong, X., Liu, L. and Qian, Y. (2021) 'Low-light image enhancement via Poisson noise aware retinex model', *IEEE Signal Processing Letters*, Vol. 31, No. 99, p.1.

Li, L., Yu, X.L., Liu, Z.L. et al. (2022) 'RFID tag group recognition based on motion blur estimation and YOLOv2 improved with the Gaussian algorithm', *Metrology and Measurement Systems: Metrologia i Systemy Pomiarowe*, Vol. 29, No. 1, pp.53–74.

Lin, Y., Ling, W.K., Xu, N. et al. (2022) 'Two dimensional quaternion valued singular spectrum analysis with application to image denoising', *Journal of the Franklin Institute*, Vol. 359, No. 8, pp.3808–3830.

Liu, J., Liu, X., Yin, Y. et al. (2022) 'Surface defect detection method of workpiece for unbalanced sample space', *Mechanical Science and Technology for Aerospace Engineering*, Vol. 41, No. 5, pp.755–763.

Luo, D., Lu, T. and Chen, Y.F. (2021) 'Application of ultra-high-performance concrete in prefabricated buildings', *Materialpruefung: Werkstoffe und Bauteile, Forschung Prufung Anwendung*, Vol. 63, No. 12, pp.74–83.

Ma, R., Li, S., Zhang, B. et al. (2022) 'Meta PID attention network for flexible and efficient real-world noisy image denoising', *IEEE Transactions on Image Processing*, Vol. 25, No. 31, pp.2053–2066.

Mahendrakar, A.K., Kumaran, S.P., Reddy, B.N. et al. (2022) 'Utility of apparent diffusion coefficient (ADC) values in differentiating benign and malignant skull lesions with histopathological (HPE) correlation', *Journal of Clinical Neuroscience: Official Journal of the Neurosurgical Society of Australasia*, Vol. 19, No. 98, pp.21–28.

Meng, X., Lu, T., Min, F. et al. (2021) 'An effective weighted vector median filter for impulse noise reduction based on minimizing the degree of aggregation', *IET Image Processing*, Vol. 15, No. 1, pp.228–238.

Panetta, K., Kezebou, L., Oludare, V. et al. (2022) 'Comprehensive underwater object tracking benchmark dataset and underwater image enhancement with GAN', *IEEE Journal of Oceanic Engineering*, Vol. 47, No. 1, pp.59–75.

Sun, Z., Li, F., Chen, W. et al. (2021) 'Underwater image processing method based on red channel prior and Retinex algorithm', *Optical Engineering*, Vol. 60, No. 9, pp.1–12.

Wang, L., Zhang, Z., Wang, Q. et al. (2022) 'Infrared image defect detection based on the algorithm of intuitionistic fuzzy C-means clustering', *Infrared Technology*, Vol. 44, No. 11, pp.1220–1227.

Yu, Y., Han, Z. and Xu, C. (2022) 'NOx concentration prediction based on deep convolution neural network and support vector machine', *Proceedings of the CSEE*, Vol. 42, No. 1, pp.238–248.

Zou, Y., Zhang, Z., Li, Q. et al. (2021) 'Crack detection and segmentation in CT images using Hessian matrix and support vector machine', *Optics and Precision Engineering*, Vol. 29, No. 10, pp.2517–2527.